

Pressure induced redistribution of oxygen hole states in $\text{La}_4\text{Ni}_3\text{O}_{10}$

Guiwen Jiang,¹ Liang Si,^{2,3} George A. Sawatzky,^{4,5} and Mi Jiang ¹

¹*School of Physical Science and Technology, Soochow University, Suzhou 215006, China*

²*School of Physics, Northwest University, Xi'an 710127, China*

³*Institute of Solid State Physics, TU Wien, 1040 Vienna, Austria*

⁴*Department of Physics and Astronomy, University of British Columbia, Vancouver BC, Canada V6T 1Z1*

⁵*Stewart Blusson Quantum Matter Institute, University of British Columbia, Vancouver BC, Canada V6T 1Z4*

Using density functional calculations and multi-orbital, multi-atom cluster exact diagonalization that includes local exchange and Coulomb interactions, we explored the local low-energy electronic states of trilayer $\text{La}_4\text{Ni}_3\text{O}_{10}$ via a minimal Ni_3O_{14} cluster. We find that, at ambient pressure, starting with all three Ni being nominally 2+ valence, one of the two extra holes is localized in the central NiO_2 layer forming a Zhang-Rice singlet (ZRS) with $d_{x^2-y^2}$ orbital. The other hole mainly occupies the antibonding combination of the two interplane O p_z orbitals and thereby hybridizes with an out-of-plane three-spin-polaron (3SP) formed by the d_{z^2} orbitals of three NiO_2 layers. In this way, the in-plane spin orientation alternation is carried by the $d_{x^2-y^2}$ orbitals of two outer layers with interlayer antiferromagnetic correlation. Simultaneously, the central layer is insulating with negligible magnetic moment. At high pressure, however, the two extra holes are concentrated on one of two outer layers and the inner layer separately forming the ZRS with $d_{x^2-y^2}$ orbitals or in-plane 3SP with neighboring cluster. We highlight the similarities between the bilayer $\text{La}_3\text{Ni}_2\text{O}_7$ and trilayer $\text{La}_4\text{Ni}_3\text{O}_{10}$ via possible charge and spin ordered states suggested by our cluster results.

I. INTRODUCTION

Recently superconductivity (SC) has been discovered in both bilayer and trilayer Ruddlesden-Popper (RP) nickelate single crystals under pressure, with maximum transition temperatures T_c of about 80 K and 30 K, respectively [1–3]. Compared to $\text{La}_3\text{Ni}_2\text{O}_7$, $\text{La}_4\text{Ni}_3\text{O}_{10}$ exhibit better sample quality and greater stability despite that its superconducting transition temperature is significantly lower than that of $\text{La}_3\text{Ni}_2\text{O}_7$, possibly due to the weaker electronic correlations in $\text{La}_4\text{Ni}_3\text{O}_{10}$ [4, 5]. With increasing pressure, the density-wave order in $\text{La}_4\text{Ni}_3\text{O}_{10}$ is suppressed, accompanied by a structural transition from the $P2_1/a$ phase to the $I4/mmm$ phase, concomitant with the emergence of SC [2, 3]. The interplay between the crystal structure, density-wave order, and SC is highly intricate. Several studies showed that several other phases or crossovers occur between the low and high pressure phases [2, 3, 6] indicating the close proximity of various electronic and magnetic structures.

Numerous experimental studies have demonstrated a close correlation between SC and density-wave order [4–6]. In $\text{La}_4\text{Ni}_3\text{O}_{10}$ microcrystals synthesized in the $I4/mmm$ phase at ambient pressure, no signature of density-wave formation or SC has been observed even under pressures up to 160 GPa [7]. This observation suggests that the density-wave order, rather than the structural transition itself, plays a crucial role in the emergence of SC. Further investigation revealed that the spin-density-wave (SDW) and charge-density-wave (CDW) components remain coupled as pressure increases [5, 6, 8]. The SDW transition exhibits a first-order-like character, and its transition temperature coincides with that of the CDW [8]. In addition, two μSR studies have reported an additional SDW order emerging at a lower temperature of $T_{\text{SDW}} \approx 80$ K in samples of

single-crystalline and polycrystalline $\text{La}_4\text{Ni}_3\text{O}_{10}$ [8, 9].

Exploring electronic structures is essential to gain the basic insight into the superconducting mechanism of $\text{La}_4\text{Ni}_3\text{O}_{10}$. Angle-resolved photoemission spectroscopy (ARPES) measurements and DFT calculations reveal that, in addition to $d_{x^2-y^2}$ orbital, $\text{La}_4\text{Ni}_3\text{O}_{10}$ also exhibits a significant $d_{3z^2-r^2}$ orbital character [10]. However, there remains considerable debate regarding which orbital plays the dominant role in SC. In particular, recent orbital-selective resonant inelastic X-ray scattering (RIXS) measurements indicate that the $d_{x^2-y^2}$ orbital dominate the low-energy charge excitations and exhibit more itinerant behavior [11]. They also observed ~ 0.1 eV bimagnon through RIXS and Raman spectroscopy, leading to an interlayer superexchange interaction J_z of ~ 50 meV [11].

Theoretical studies based on density functional theory combined with dynamical mean-field theory (DFT+DMFT) have extensively investigated the electronic correlations and the role of Hund's coupling in $\text{La}_4\text{Ni}_3\text{O}_{10}$ [12, 13]. Another DFT+DMFT simulation has shown that the inner/outer NiO_2 layer possesses weak/strong Hund correlation [14]. Several theoretical studies based on random phase approximation (RPA) have suggested that this system predominantly supports the s^\pm -wave pairing [15, 16], consistent with the conclusion obtained from the minimal tight-binding model [17]. In addition, DFT+U calculations under pressure have revealed an upward shift of the $\text{Ni-}d_{3z^2-r^2}$ bonding band and a reconstruction of the electronic states, while RPA and multi-orbital analysis emphasized the role of $d_{x^2-y^2}$ magnetism and charge-transfer character [18].

Compared with $\text{La}_3\text{Ni}_2\text{O}_7$, $\text{La}_4\text{Ni}_3\text{O}_{10}$ possesses additional orbital and layer degrees of freedom, making many numerical approaches computationally challenging.

Although exact diagonalization (ED) is constrained to small clusters, thus introducing finite-size effects, its significance lies in producing numerically exact solutions. It avoids the sign problem that limits methods such as determinant quantum Monte Carlo (DQMC) and allows for the direct computation of zero-temperature ground and excited states. This precision, combined with the relative ease of incorporating complex interactions such as those in multi-orbital systems with Hund's coupling, establishes ED as a critical benchmark for theories of strong correlation. The remainder of this paper is organized as follows. In Section II, we introduce the DFT calculation and the multi-orbital cluster model. Section III presents the numerical results and analysis. Finally, in Section IV with a summary and discussion.

II. MODEL AND METHODOLOGY

A. DFT calculations and Wannier projections

The Density-functional theory [19, 20] level structural relaxations and band structure calculations were performed using the VASP [21, 22] and WIEN2K [23, 24] codes with the Perdew-Burke-Ernzerhof version of the generalized gradient approximation (GGA-PBE) [25] and a dense of over 2000 k -points for the unit cell of $\text{La}_4\text{Ni}_3\text{O}_{10}$. The parameters listed in Table I are determined from the corresponding DFT Bloch bands and Maximally localized Wannier functions [26, 27] projections using WANNIER90 [28] and WIEN2WANNIER [29] interface. The most crucial parameters in all three models are the hybridization tds between Ni- $3d_{x^2-y^2}$, Ni- $3d_{z^2}$ and in-plane and apical O- $2p$ orbitals, and these hopping parameters between Ni- $3d$ orbitals, Ni- $3d$ /O- $2p$ to O- $2p$ were obtained via the Wannier projections for models of Ni- $3d$ subspace and Ni- $3d$ and O- $2p$ substate, respectively.

The hole hopping parameters for the $P2_1/a$ phase at 0 GPa and the $I4/mmm$ phase at 15.3 GPa are listed in Table I.

B. Multi-orbital cluster Model

Here we extend our previous study [30] of the bilayer Ni_2O_9 cluster to a trilayer Ni_3O_{14} cluster comprising three NiO_2 planes separated by apical oxygen atoms as depicted in Fig. 1. As shown before [30], the bilayer cluster indicated that 4 of the totally 5 holes occupy the two Ni $3d^8$ sites and the remaining hole mainly occupies the in-plane O p_x orbitals. Because of the local nature of this minimal cluster, we focus on the intrinsic local physics induced by the interplay of the hybridization between various orbitals and interactions among these orbitals.

Assuming a fixed -2 valence for oxygen, the total formal valence of the three Ni ions in $\text{La}_4\text{Ni}_3\text{O}_{10}$ sums

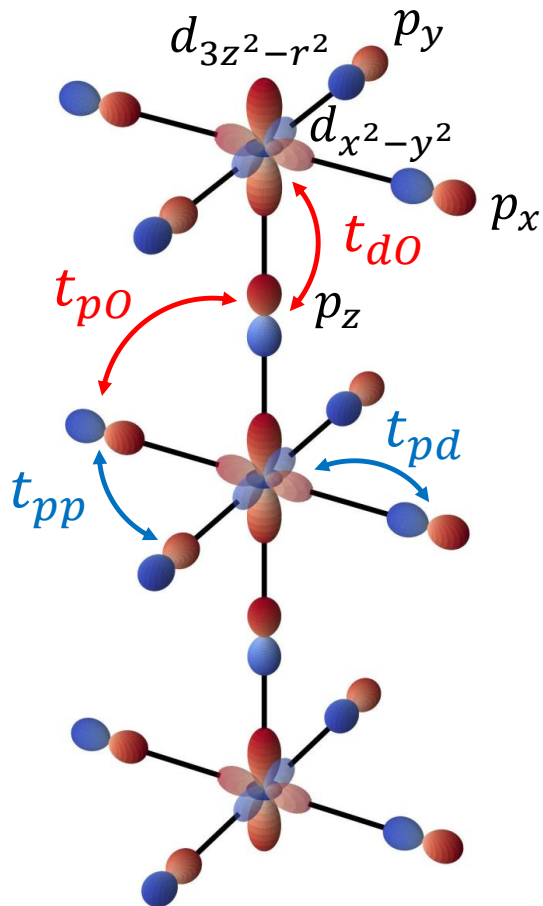


FIG. 1. Geometry of the Ni_3O_{14} cluster used in the calculations. The figure shows the Ni and O orbitals retained in the configuration basis and the Ni-O and O-O hopping paths included in the model Hamiltonian.

up to $+8$, producing an average Ni valence of $+2.67$, commonly described as a mixture of Ni^{2+} and Ni^{3+} . However, compared to the bilayer $\text{La}_3\text{Ni}_2\text{O}_7$, the hole distribution in this trilayer system is considerably more complex. Presumably, in the hole language adopted in our previous work [30], 6 of 8 holes would occupy the three Ni $3d^8$ sites so that the key question is where the remaining two holes locate among different layers and orbitals, which is largely affected by the pressure induced change of various hybridization.

We employ the exact diagonalization calculation of the Hamiltonian

$$\mathcal{H} = \hat{E}_d + \hat{E}_p + \hat{E}_O + \hat{T}_{pp} + \hat{T}_{dp} + \hat{T}_{do} + \hat{T}_{po} + \hat{U}_{dd} + \hat{U}_{pp} + \hat{U}_{OO} \quad (1)$$

where \hat{E}_d , \hat{E}_p and \hat{E}_O are the on-site energies for the orbitals of Ni, the oxygen ligand $2p$, and the inter-layer apical oxygen. As usual, the site energy of Ni- $3d_{x^2-y^2}$ is set to zero as a reference. Here, \hat{T}_{pp} , \hat{T}_{dp} , \hat{T}_{do} and \hat{T}_{po}

TABLE I. On-site energies ϵ , Racah parameters A, B, C , and hopping integrals T_{mn}^{pd} with $m \in \{d_{x^2}, d_{z^2}\}$ with $d_{x^2} \equiv d_{x^2-y^2}$ and $d_{z^2} \equiv d_{3z^2-r^2} = d_{2z^2-(x^2+y^2)}$ respectively and $n \in \{p_x, p_y\}$, where m, n are nearest neighbors, extracted from DFT calculations. Note that we only consider p_x and p_y orbitals for in-plane O denoted by p with lobes pointing to the Ni ion; while only the p_z orbital is considered for the interlayer apical Oxygen denoted by O .

$T_{x^2-y^2,n}^{pd}$	$T_{z^2,n}^{pd}$	e_{dx^2}	A	B	C	U_{OO}	U_{pp}
t_{pd}	$t_{pd}/\sqrt{3}$	0	6	0.15	0.58	4.0	4.0
<hr/>							
0 GPa	e_{dz^2}	e_p	e_O	t_{pd}	t_{pp}	t_{do}	t_{po}
Inner	0.02	2.875	2.76	1.285	0.435	1.210	0.435
Outer	0.17	3.093	/	1.187	0.478	1.266	0.403
<hr/>							
15.3 GPa	e_{dz^2}	e_p	e_O	t_{pd}	t_{pp}	t_{do}	t_{po}
Inner	-0.076	3.364	3.047	1.503	0.525	1.625	0.489
Outer	0.116	3.519	/	1.498	0.551	1.666	0.486

describe the hopping integrals between the inter-layer apical oxygen (O), considered only via its p_z orbital, and the Ni- $3d_{3z^2-r^2}$ and O- $2p$ in-plane ligand orbitals. The symbol L refers to a linear combination adapted to the symmetry of the four orbitals of the nearest-neighbor O ligand, which hybridizes with a specific Ni $3d$ orbital. For example, the $x^2 - y^2$ and $3z^2 - r^2$ symmetries hybridize with the $3d_{x^2-y^2}$ and $3d_{3z^2-r^2}$ orbitals, respectively. \hat{U}_{dd} , \hat{U}_{pp} , and \hat{U}_{OO} describe their on-site Coulomb interactions respectively [31]. Specifically, \hat{U}_{dd} is the Coulomb and exchange integrals corresponding to the symmetry D_{4h} in terms of Racah parameters A, B, C , which are connected to the Slater integrals F^0 , F^2 , and F^4 for the transition metal $3d^8$ multiplets as [32]

$$\begin{aligned}
 A &= F^0 - \frac{49}{441} F^4 \\
 B &= \frac{1}{49} F^2 - \frac{5}{441} F^4 \\
 C &= \frac{35}{441} F^4
 \end{aligned} \tag{2}$$

The parameter A is analogous to the Hubbard U commonly referenced in nickelate, while B and C , derived from atomic physics, quantify the energy differences for the two holes in the Ni $3d$ shell, including their dependence on the relative spin and orbital orientation. The conventional Racah parameters for Ni, with $A = 6.0$ eV, $B = 0.15$ eV, and $C = 0.58$ eV are adopted similar to our previous work [33]. The DFT calculations indicate that low-energy physics is dictated by the Ni e_g orbitals. Hence, our Hilbert space is restricted to these two Ni e_g orbitals and the O- $2p$ orbitals that hybridize with them through σ bonds (as shown in Fig. 1).

Furthermore, the on-site Hubbard interaction for two holes in the same oxygen atom has been measured by Auger spectroscopy in oxides, generating a value of 4.6 eV in Cu_2O [34]. Given the relatively smaller ionic size of Ni, we adopt an estimated value of 4.0 eV for both the apical and in-plane oxygen sites.

To denote the multi-hole configuration, throughout our work, the notation like $d^7-d^8-O-d^8$ refers to the configuration that the three Ni layers as d^7 , d^8 , and d^8

states with O specifying the interlayer apical oxygen. For example, the configuration $d^8-d^8L-O-d^8$ plays a significant role in our following discussion. Such an asymmetric configuration apparently has its mirror configuration $d^8-O-d^8L-d^8$, whose weight contribution will be incorporated into the total wave function but still denoted by $d^8-d^8L-O-d^8$. Putting another way, the two interlayer apical O's p_z orbitals can form the bonding and antibonding combination with energy splitting between them. Our simulations at low pressure uncovered that the antibonding combination ($d^8-d^8L-O-d^8$ minus $d^8-O-d^8L-d^8$) is the the lowest energy state, which hybridizes with all three d_{z^2} orbitals because of their phases. Upon increasing pressure, a phase transition occurs, and the dominant configuration becomes $d^8-d^8L-d^8L$.

Besides, for d^8 states involving $d_{z^2}d_{x^2}$, the curly braces $\{.\}$ and square brackets $[.]$ are used to indicate spin pairs coupled in triplet and singlet states respectively. The shorthands $x = d_{x^2} \equiv d_{x^2-y^2}$ and $z = d_{z^2} \equiv d_{3z^2-r^2}$ are adopted, and S represents the total spin for the various 7, 8 and 9 holes states of the cluster, which is a good quantum number for our cluster model.

C. Energy level diagram

Before solving the Ni_3O_{14} cluster, we first consider the atomic limit to determine the hole distribution and the corresponding energies. Similar to $\text{La}_3\text{Ni}_2\text{O}_7$, the building block of $\text{La}_4\text{Ni}_3\text{O}_{10}$ is d^8 , which is taken as the energy reference.

We start from the definition of the Hubbard interaction

$$U = E(d^{n+1}) + E(d^{n-1}) - 2E(d^n) \tag{3}$$

and the onsite energy of the d orbital in the hole language

$$\epsilon_d = E(d^9) - E(d^{10}) \tag{4}$$

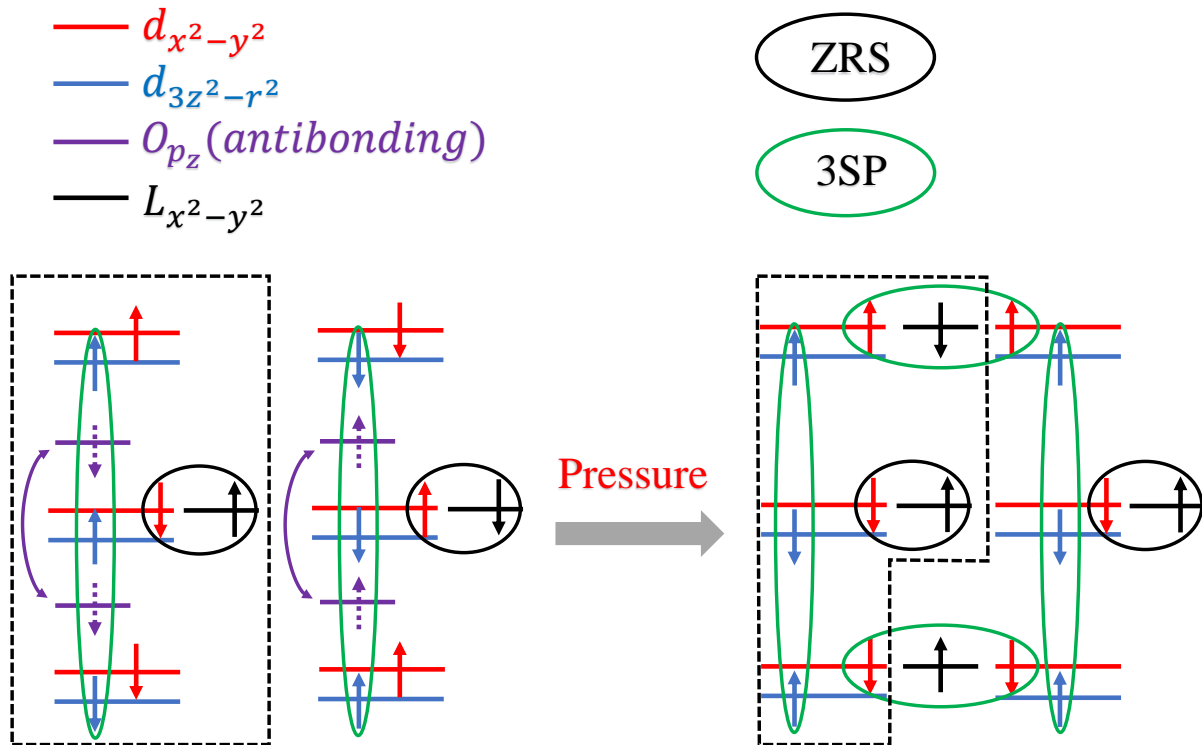


FIG. 3. Schematic diagram of the two neighboring 8-hole clusters (black dashed box) illustrating the pressure induced redistribution of the oxygen hole states. At ambient pressure, apart from the Zhang-Rice singlet (ZRS) in the central layer, the other hole locates on the antibonding combination of two interlayer apical oxygens and thereby couples with the 3-spin-polaron (3SP) formed by three d_{z^2} orbitals. At high pressure, this hole reverts to the outer layers and forms an in-plane 3SP with the neighboring cluster.

central z spin is antiferromagnetically coupled with each of the outer layer z spins via superexchange. This out-of-plane 3SP has different nature from the conventional in-plane 3SP involving O- $2p$ and Ni- x that has much larger antiferromagnetic exchange [37].

We remark that the physical picture in Fig. 3 is based on our concrete calculation of a single isolated minimal cluster consisting of 8 holes together with reasonable extension to two neighboring cluster. More involved calculation explicitly considering the inter-cluster interaction is formidable and out of the scope of the current research.

In what follows, we will provide more details on our numerical calculations. Our investigation spans over a broad range of hybridizations highlighting the physics near the DFT-derived parameters (labeled as red stars in the figures). The GS nature is governed by the competition among the Hund's coupling, the x - p exchange through t_{pd} , and the z - p_z exchange via t_{dO} . In addition, we have the interlayer z - z superexchange that is active in the case of no holes in the intervening p_z orbital. To examine the effect of hybridization, the ratio t_{dO}/t_{pd} is fixed as the DFT value at each pressure, while t_{pd} ranges from 0.9 to 1.1 times its DFT value.

A. GS weight distribution: 8-hole system

Fig. 4 compares the weight distribution with t_{pd} of the GS between 0 GPa and 15.3 GPa, which exhibit qualitatively distinct features. At ambient pressure (red star of panel a), the dominant configuration is $d^8-d^8L-O-d^8$, where each layer hosts one d^8 state and the two remaining holes reside in the in-plane and apical oxygen respectively. The L hole on in-plane oxygen has $x^2 - y^2$ symmetry to form a Zhang-Rice singlet (ZRS) (well known in hole-doped cuprates) with the Ni- x orbital. As already shown in the left panel of Fig. 3, the inter-layer z - z - z 3SP hybridizes with the antibonding combination of two interlayer apical p_z orbitals. We have determined that the total spin of this out-of-plane 3SP is 1/2. The strong hybridization with the antibonding O- p_z so that the large exchange interaction decouples the z spins from the x orbital on the same Ni, i.e. the Hund's rule coupling is strongly suppressed because of the "dilution" effect.

To consider the possible ambiguity of the parameters in the realistic solid circumstances, we tuned t_{pd} (with fixed ratio t_{pd}/t_{dO}) in Fig. 4 and uncovered that a phase transition occurs such that the dominant configuration becomes $d^8-d^8L-d^8L$. In other words, if simply treating enlarged t_{pd} as a way of mimicking the high pressure, the

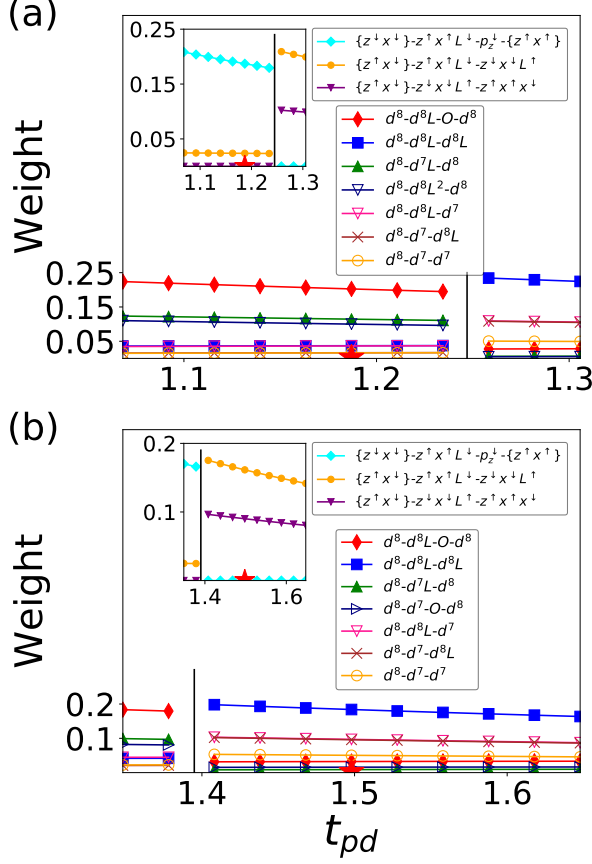


FIG. 4. Comparison of GS weight distribution with t_{pd} at fixed ratio t_{pd}/t_{dO} between (a) ambient and (b) 15.3 GPa pressure. The red star denotes the DFT parameters. The \cdot and $[\cdot]$ symbols denote two hole spins forming triplet and singlet states respectively. The inset provides more details on the leading configurations. The $d_{3z^2-r^2}$ and $d_{x^2-y^2}$ orbitals are labeled as z and x for simplicity.

x - $L_{x^2-y^2}$ hybridization becomes increasingly dominant, driving the transfer of hole from the apical O site to in-plane O sites forming two in-plane ZRS as already shown in the right panel of Fig. 3. Besides, note that these two ZRS locate on the inner and outer layer separately. This brings us to a situation similar to that of the bilayer RP nickelates, namely that the in-plane hole in the outer layers can be in phase or out of phase since its density is one per two in-plane Ni.

At high pressure (Fig. 4(b)), a phase transition appears again but to the left of the red star. Combined with the transition in Fig. 4(a), it strongly suggests the presence of a phase transition between the ambient and high pressure. This also further indicates that varying t_{pd} while keeping the ratio t_{dO}/t_{pd} fixed provides a reasonable way to simulate the pressure effect.

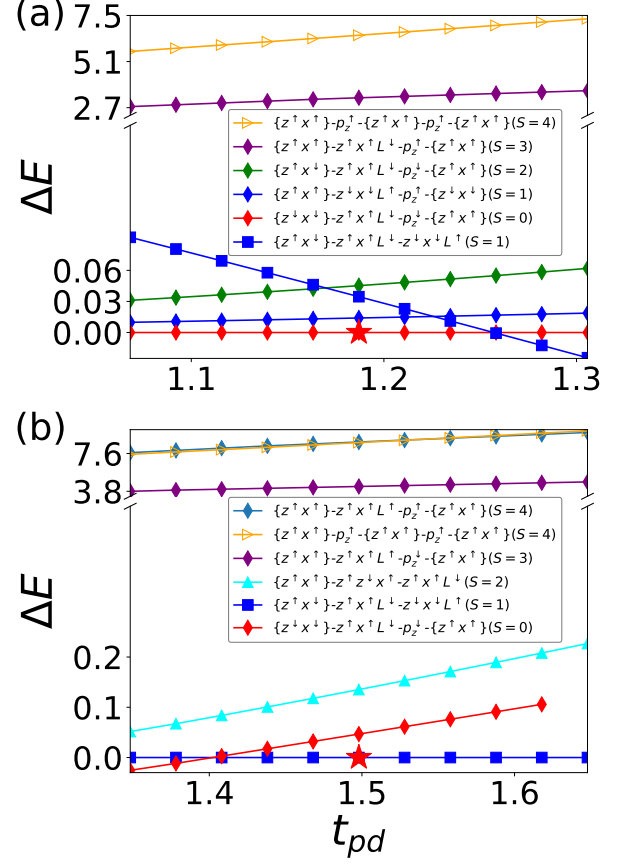


FIG. 5. Excited energy splittings between spin multiplets relative to the ground state as a function of t_{pd} at fixed t_{pd}/t_{dO} for (a) ambient and (b) 15.3 GPa pressure. The red star denotes the DFT parameters. Labels indicates the dominant configurations and their corresponding total spins.

B. Spin state analysis of 8-hole system

The pressure induced phase transition between two dominant configurations revealed in Fig. 4 leads to the total spin change as well. At ambient pressure, shown in Fig. 5(a), the low-lying eigenstates with different total spins are closely spaced in energy. In particular, the energy gaps between the $S = 0, 1, 2$ are quite small. This arises from the dominant $d^8-d^8L-O-d^8$ configuration, where the $d_{x^2-y^2}$ orbital within d^8L forms an in-plane ZRS with the ligand L hole, leaving an unpaired spin- $\frac{1}{2}$ in the z orbital forming 3SP with another two z orbitals of the outer layers and in turn hybridizes with the antibonding p_z orbital of the bridging interlayer apical O. As shown in left part of Fig. 3, this subsystem of out-of-plane 3SP together with the antibonding p_z hole induces a weak exchange between the two outer layers. The superexchange between the outer layers is smaller than that of the bilayer 327 compound. This smaller superexchange is likely the cause of the lower T_c . In

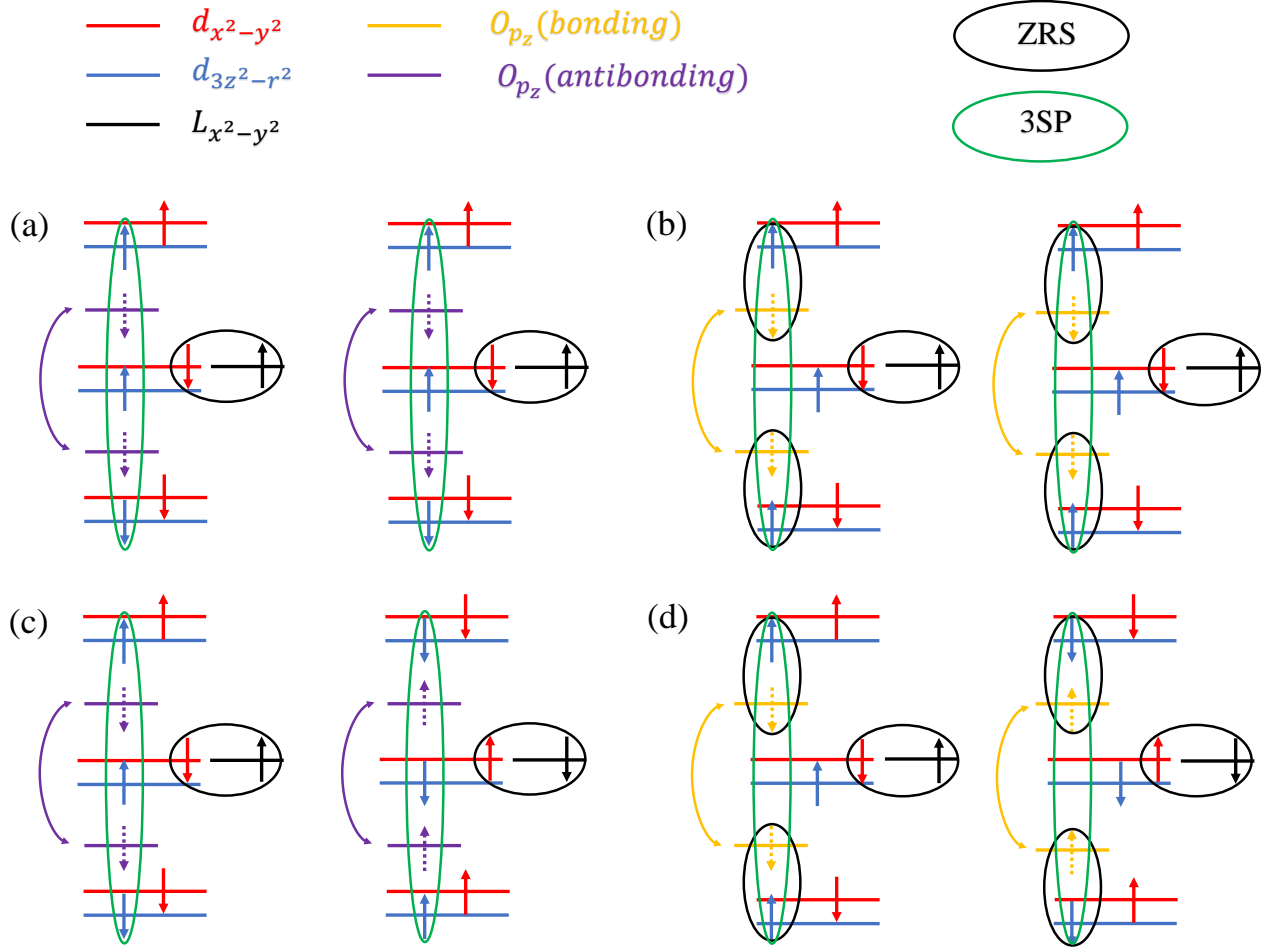


FIG. 6. Possible configurations of two neighboring clusters at ambient pressure with (a-b) spin parallel and (c-d) spin opposite between clusters. The right panels (b,d) show the bonding combination case of two interlayer apical O in spite of its higher energy than the antibonding combinations of right panels (a,c).

fact, the superexchange between two outer layers are small, which is reflected by the small energy gaps between different spin states in Fig. 5.

In contrast, for $S = 3$ and $S = 4$, the ZRS is broken, leading to Zhang-Rice triplet like configurations with ferromagnetic spin alignment, resulting in a substantial increase in the total energy. In addition, the energy splittings between $S = 0, 1, 2$ configurations are so small that it allows for spin state transition, as observed in the GS spin changes from $S = 0$ at ambient pressure to $S = 1$ at large t_{pd} , which is consistent with the phase transition around $t_{pd} \sim 1.25$ in Fig. 4(a). These observations would lead to additional phase transitions or crossovers, as observed experimentally.

Moving to Fig. 5(b), clearly there is also a transition from GS $S = 0$ to $S = 1$ around $t_{pd} \sim 1.4$ mirroring the transition in Fig. 4(b). Interestingly, although the GS at 0 and 15.3 GPa differ markedly in both spin and orbital configuration, the excited states in both cases show a similar evolution, from configurations dominated by in-plane oxygen holes to those involving inter-layer

apical oxygens and eventually forming the $d^8-O-d^8-O-d^8$ pattern at very high-energy $S = 3, 4$ states.

Fig. 3 only illustrates one reasonable configuration of two neighboring clusters. Because Fig. 5(a) reveals the quite small energy difference between various configurations of different total spins, for example, the blue and red diamond curves, this strongly implies that adding into inter-cluster interaction, albeit out of our current simulation capability, could radically change the configurations shown in Fig. 3 obtained via our isolated simulations. Therefore, more possibilities for the ambient pressure are shown in Fig. 6, where the upper/lower panel shows the spin parallel/opposite between clusters, respectively. Note that either situation does not contradict the experimentally revealed spin density wave vector [39, 40]. In addition, the panels (b) and (d) also provide the pictures of bonding combination of two interlayer apical Oxygens, although their weight in GS is much smaller than their antibonding counterparts shown as panel (a) and (c). In other words, the bonding combination has much higher energy than the

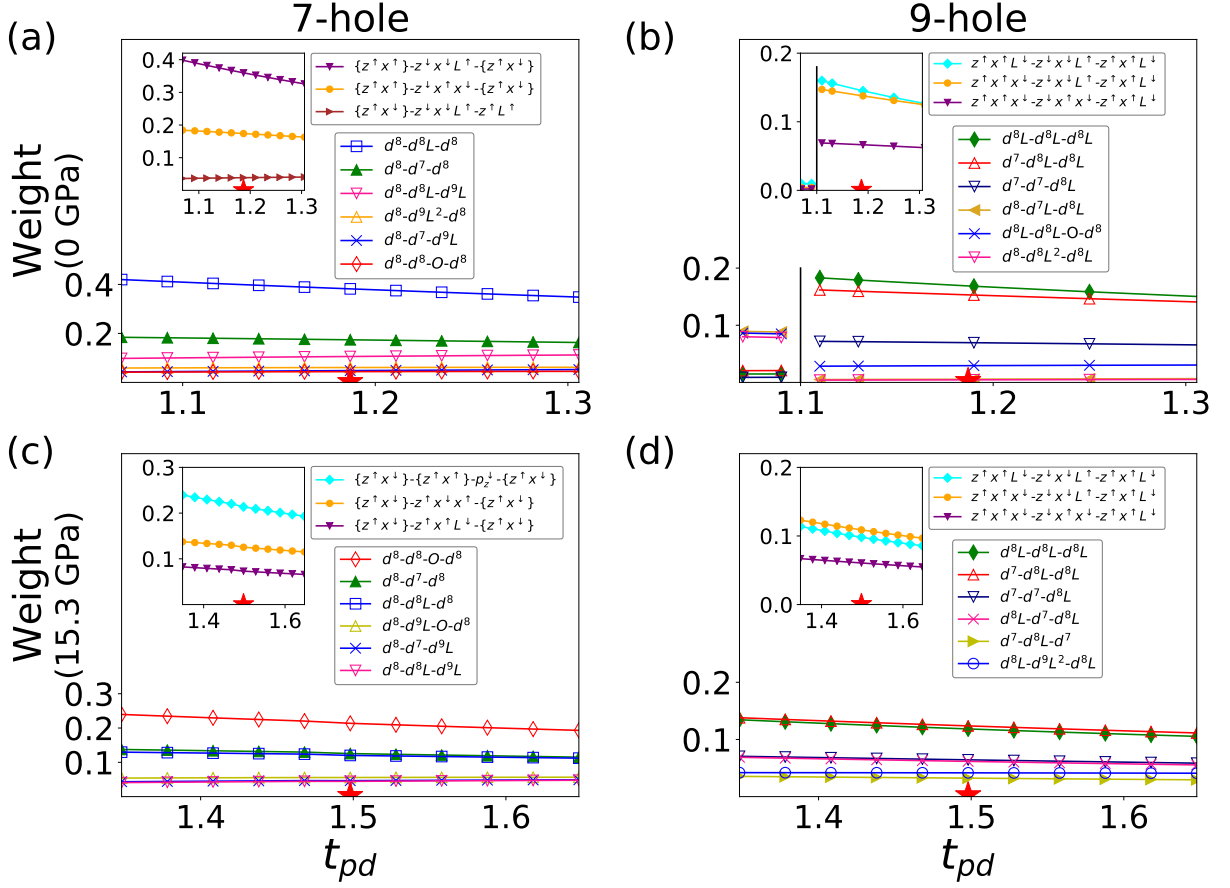


FIG. 7. GS weight distribution of 7-hole and 9-hole system for both ambient and high pressure.

antibonding case focused in the present study e.g. Fig. 3. This observation emphasizes the importance of the z orbital of the central layer, which plays a vital role in bridging two outer layers.

C. 7- and 9-hole systems

In our previous investigation on bilayer $\text{La}_3\text{Ni}_2\text{O}_7$ [30], we have seen the possible role of charge density modulation between two neighboring clusters. Similar analysis can be performed for the trilayer $\text{La}_4\text{Ni}_3\text{O}_{10}$. To this aim, we first discuss the GS weight distribution of the 7- and 9-hole systems, which are electron addition and removal states separately and closely related to the conductivity gap of the 8-hole system. Precisely, the gap is the energy difference $\Delta E = E_{7+9} - E_{8+8}$ between the GS energy of a 7- and a 9-hole clusters $E_{7+9} = E_{GS,7} + E_{GS,9}$ and that of two 8-hole clusters, $E_{8+8} = 2E_{GS,8}$. We found that the effective conductivity gap turns out to be small, which is well within the expected bandwidth due to the inter-cluster hopping. Hence, these materials are predicted to be metals although small gaps could occur if indeed spin and charge density waves exist, which

is out of our capability to decisively determine that.

Fig. 7 illustrates the pressure dependence of their GS weights of the dominant configurations. For 7-hole system, starting from the d^8 states in all three layers, the high pressure induces the transition to the dominant configuration of the extra hole occupying apical O (panel c) from the in-plane O at ambient pressure (panel a).

For 9-hole system, unless for very small t_{pd} , the physically relevant DFT parameters at both ambient (panel b) and high pressure (panel d) result in the leading configuration of d^8L in all three layers with strong involvement of d^7 state in one outer layer. Nonetheless, the apical O only plays a minor role in 9-hole system.

With the above manifestation of 7- and 9-hole system combining with the previously discussed 8-hole one, we can speculate on more possible ordered phases suggested by these single cluster results. Specifically, Fig. 3 only illustrates the situation of two neighboring clusters both with 8 holes. Instead, Fig. 8 reveals other possibilities consisting of 7+9 holes. Intriguing, the ambient pressure configuration is the same as the high pressure case of 8+8 holes, namely in-plane 3SP within two outer layers. At high pressure, all three layers possess the in-plane 3SP as well as the presence of antibonding apical O.

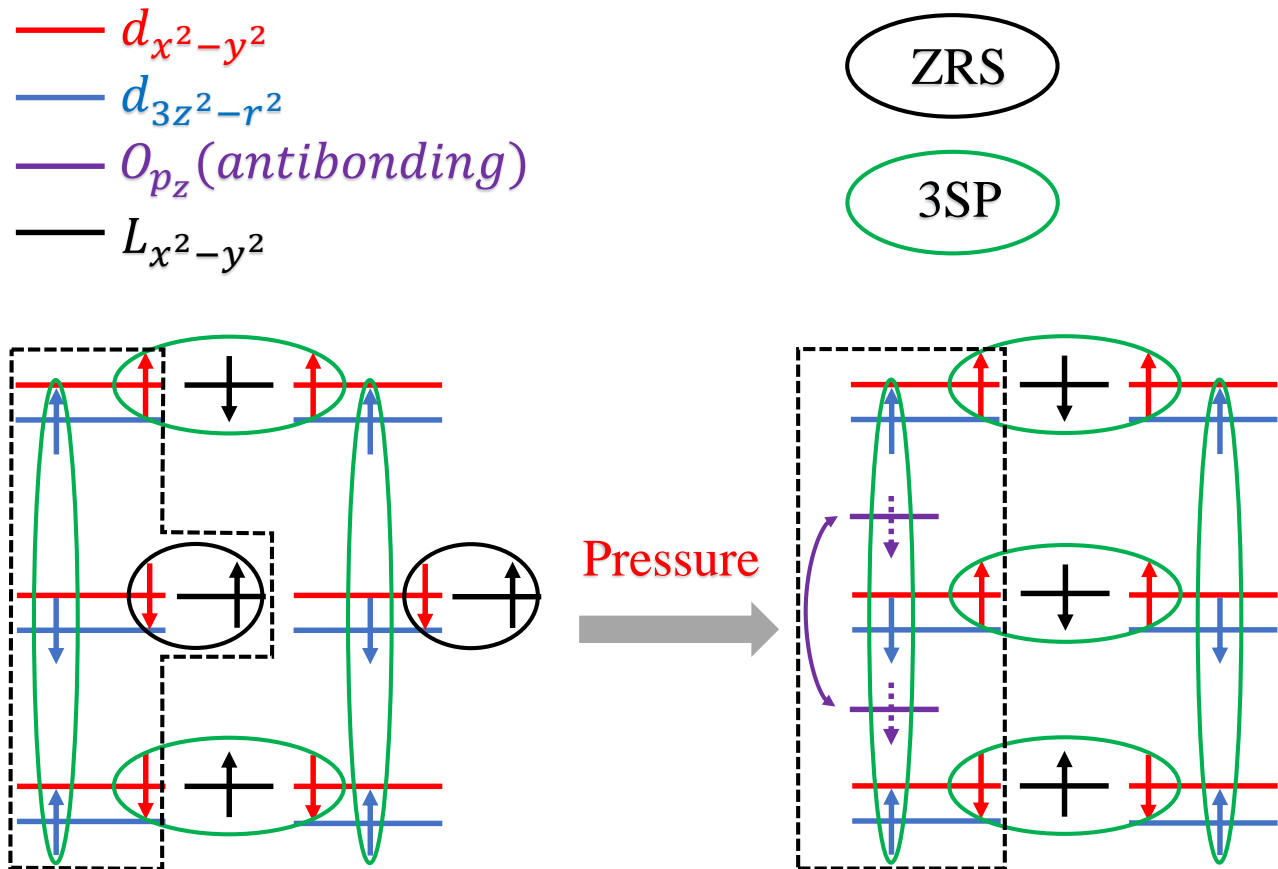


FIG. 8. Schematic diagram of neighboring 7-hole (black dashed box) and 9-hole clusters illustrating the possible pressure induced redistribution of the oxygen hole states.

All possible configurations of two neighboring clusters (either 7+9 holes or 8+8 holes) can be categorized by the number N_{3SP} of in-plane 3SP states: (i) $N_{3SP} = 0$ as shown in Fig. 3's left side; (ii) $N_{3SP} = 2$ and locate on two outer layers as shown in Fig. 8's left side; (iii) $N_{3SP} = 3$ evenly distributed on all layers as shown in Fig. 8's right side.

IV. SUMMARY AND OUTLOOK

In summary, the present study reveals that the undoped $\text{La}_4\text{Ni}_3\text{O}_{10}$ exhibits markedly different characteristic between ambient and high pressure. Specifically, starting with all three Ni being nominally 2+ valence, at ambient pressure, the GS is dominated by configurations with one of the extra two holes preferentially confined in the central layer's in-plane O 2p orbitals coupling with the x orbital as a Zhang-Rice singlet; while the other hole locates on the antibonding combination of two interlayer apical oxygens and thereby couples with the 3-spin-polaron (3SP) formed by three z orbitals. In addition, the left side of Fig. 3 also reveals the in-plane spin orientation alternation carried by the two outer layers with interlayer

antiferromagnetic correlation. Concurrently, the central layer is insulating, which is similar to what happens in the 113 nickelates like NdNiO_3 [38] and nearly nonmagnetic. These observations are all consistent with the recent experiments [39].

On the contrary, under high pressure, the apical O contribution vanishes and two additional holes both locate into two neighboring NiO_2 layers. In particular, one hole resides on the in-plane Oxygen of the outer layers and forms a in-plane 3SP with the neighboring cluster. Therefore, the net result is one hole per two in-plane O of outer layers as in the case of $\text{La}_3\text{Ni}_2\text{O}_7$ but now in addition to one hole in $x^2 - y^2$ symmetry per Ni in the central layer. Concurrently, similar to the ambient pressure situation, three z orbitals form an 3SP where the central z spin is antiferromagnetically coupled with each of the outer layer z spins via superexchange. This out-of-plane 3SP has different nature from the convention in-plane 3SP involving O-2p and Ni- x that has much larger antiferromagnetic exchange [37].

Our findings are based on our concrete calculation of a single isolated minimal cluster consisting of 8 holes together with reasonable extension to two neighboring cluster. More involved calculation explicitly considering the inter-cluster interaction, in spite of its

formidable complexity, is strongly desired in future research to uncover more distinct physics in this nickelate superconductor.

V. ACKNOWLEDGMENTS

Guiwen Jiang and Mi Jiang acknowledge the support of the National Natural Science Foundation of China (Grant

No.12174278). Liang Si acknowledges support from the National Natural Science Foundation of China (Grant No.12422407). George A. Sawatzky is supported by the Quantum Matter Institute (QMI) at the University of British Columbia and the Natural Sciences and Engineering Research Council of Canada (NSERC). The computational work was carried out on the resources provided by Soochow University and the National Supercomputing Center in Xi'an, hosted by Northwest University.

-
- [1] H. Sun, M. Huo, X. Hu, J. Li, Z. Liu, Y. Han, L. Tang, Z. Mao, P. Yang, B. Wang, *et al.*, Signatures of superconductivity near 80 K in a nickelate under high pressure, *Nature* **621**, 493 (2023).
- [2] Y. Zhu, D. Peng, E. Zhang, B. Pan, X. Chen, L. Chen, H. Ren, F. Liu, Y. Hao, N. Li, *et al.*, Superconductivity in pressurized trilayer $\text{La}_4\text{Ni}_3\text{O}_{10-\delta}$ single crystals, *Nature* **631**, 531 (2024).
- [3] M. Zhang, C. Pei, D. Peng, X. Du, W. Hu, Y. Cao, Q. Wang, J. Wu, Y. Li, H. Liu, *et al.*, Superconductivity in trilayer nickelate $\text{La}_4\text{Ni}_3\text{O}_{10}$ under pressure, *Physical Review X* **15**, 021005 (2025).
- [4] S. Xu, C.-Q. Chen, M. Huo, D. Hu, H. Wang, Q. Wu, R. Li, D. Wu, M. Wang, D.-X. Yao, *et al.*, Origin of the density wave instability in trilayer nickelate $\text{La}_4\text{Ni}_3\text{O}_{10}$ revealed by optical and ultrafast spectroscopy, *Physical Review B* **111**, 075140 (2025).
- [5] M. Li, J. Gong, Y. Zhu, Z. Chen, J. Zhang, E. Zhang, Y. Li, R. Yin, S. Wang, J. Zhao, *et al.*, Direct visualization of an incommensurate unidirectional charge density wave in $\text{La}_4\text{Ni}_3\text{O}_{10}$, *Physical Review B* **112**, 045132 (2025).
- [6] S. Xu, H. Wang, M. Huo, D. Hu, Q. Wu, L. Yue, D. Wu, M. Wang, T. Dong, and N. Wang, Collapse of density wave and emergence of superconductivity in pressurized- $\text{La}_4\text{Ni}_3\text{O}_{10}$ evidenced by ultrafast spectroscopy, *Nature Communications* **16**, 7039 (2025).
- [7] M. Shi, Y. Li, Y. Wang, D. Peng, S. Yang, H. Li, K. Fan, K. Jiang, J. He, Q. Zeng, *et al.*, Absence of superconductivity and density-wave transition in ambient-pressure tetragonal $\text{La}_4\text{Ni}_3\text{O}_{10}$, *Nature Communications* **16**, 2887 (2025).
- [8] R. Khasanov, T. J. Hicken, I. Plokhikh, V. Sazgari, L. Keller, V. Pomjakushin, M. Bartkowiak, S. Królak, M. J. Winarski, J. A. Krieger, *et al.*, Identical suppression of spin and charge density wave transitions in $\text{La}_4\text{Ni}_3\text{O}_{10}$ by pressure, *arXiv preprint arXiv:2503.04400* (2025).
- [9] Y. Cao, A. Liu, B. Wang, M. Zhang, Y. Qi, T. J. Hicken, H. Luetkens, Z. Fu, J. S. Gardner, J. Zhao, *et al.*, Complex spin-density-wave ordering in $\text{La}_4\text{Ni}_3\text{O}_{10}$, *arXiv preprint arXiv:2503.14128* (2025).
- [10] H. Li, X. Zhou, T. Nummy, J. Zhang, V. Pardo, W. E. Pickett, J. F. Mitchell, and D. S. Dessau, Fermiology and electron dynamics of trilayer nickelate $\text{La}_4\text{Ni}_3\text{O}_{10}$, *Nature communications* **8**, 704 (2017).
- [11] S. Zhang, H. Zhang, Z. Dong, J. Li, Q. Xiao, M. Huo, H.-Y. Huang, D.-J. Huang, Y. Wang, Y. Lu, *et al.*, Distinct orbital contributions to electronic and magnetic structures in $\text{La}_4\text{Ni}_3\text{O}_{10}$, *arXiv preprint arXiv:2509.20727* (2025).
- [12] Z. Huo, P. Zhang, Z. Zhang, D. Duan, and T. Cui, Electronic correlations and hund's rule coupling in trilayer nickelate $\text{La}_4\text{Ni}_3\text{O}_{10}$, *Science China Physics, Mechanics & Astronomy* **68**, 127411 (2025).
- [13] P.-F. Tian, H.-T. Ma, X. Ming, X.-J. Zheng, and H. Li, Effective model and electron correlations in trilayer nickelate superconductor $\text{La}_4\text{Ni}_3\text{O}_{10}$, *Journal of Physics: Condensed Matter* **36**, 355602 (2024).
- [14] J.-X. Wang, Z. Ouyang, R.-Q. He, and Z.-Y. Lu, Non-fermi liquid and hund correlation in $\text{La}_4\text{Ni}_3\text{O}_{10}$ under high pressure, *Physical Review B* **109**, 165140 (2024).
- [15] Y. Zhang, L.-F. Lin, A. Moreo, T. A. Maier, and E. Dagotto, Prediction of s^\pm -wave superconductivity enhanced by electronic doping in trilayer nickelates $\text{La}_4\text{Ni}_3\text{O}_{10}$ under pressure, *Phys. Rev. Lett.* **133**, 136001 (2024).
- [16] M. Zhang, H. Sun, Y.-B. Liu, Q. Liu, W.-Q. Chen, and F. Yang, s^\pm -wave superconductivity in pressurized $\text{La}_4\text{Ni}_3\text{O}_{10}$, *Physical Review B* **110**, L180501 (2024).
- [17] Q.-G. Yang, K.-Y. Jiang, D. Wang, H.-Y. Lu, and Q.-H. Wang, Effective model and s^\pm -wave superconductivity in trilayer nickelate $\text{La}_4\text{Ni}_3\text{O}_{10}$, *Physical Review B* **109**, L220506 (2024).
- [18] C.-Q. Chen, Z. Luo, M. Wang, W. Wú, and D.-X. Yao, Trilayer multiorbital models of $\text{La}_4\text{Ni}_3\text{O}_{10}$, *Phys. Rev. B* **110**, 014503 (2024).
- [19] P. Hohenberg and W. Kohn, Inhomogeneous electron gas, *Phys. Rev.* **136**, B864 (1964).
- [20] W. Kohn and L. J. Sham, Self-consistent equations including exchange and correlation effects, *Phys. Rev.* **140**, A1133 (1965).
- [21] G. Kresse and J. Furthmüller, Efficiency of ab-initio total energy calculations for metals and semiconductors using a plane-wave basis set, *Comput. Mater. Sci.* **6**, 15 (1996).
- [22] G. Kresse and J. Furthmüller, Efficient iterative schemes for ab initio total-energy calculations using a plane-wave basis set, *Phys. Rev. B* **54**, 11169 (1996).
- [23] P. Blaha, K. Schwarz, G. Madsen, D. Kvasnicka, and J. Luitz, Wien2k, an augmented plane wave+ local orbitals program for calculating crystal properties., *WIEN2k,an augmented plane wave+ local orbitals program for calculating crystal properties* (2001).
- [24] K. Schwarz, P. Blaha, and G. K. Madsen, Electronic structure calculations of solids using the wien2k package for material sciences, *Computer physics communications* **147**, 71 (2002).

- [25] J. P. Perdew, K. Burke, and M. Ernzerhof, Generalized gradient approximation made simple, *Phys. Rev. Lett.* **77**, 3865 (1996).
- [26] G. H. Wannier, The structure of electronic excitation levels in insulating crystals, *Phys. Rev.* **52**, 191 (1937).
- [27] N. Marzari, A. A. Mostofi, J. R. Yates, I. Souza, and D. Vanderbilt, Maximally localized wannier functions: Theory and applications, *Rev. Mod. Phys.* **84**, 1419 (2012).
- [28] A. A. Mostofi, J. R. Yates, Y.-S. Lee, I. Souza, D. Vanderbilt, and N. Marzari, wannier90: A tool for obtaining maximally-localised wannier functions, *Computer Physics Communications* **178**, 685 (2008).
- [29] J. Kuneš, R. Arita, P. Wissgott, A. Toschi, H. Ikeda, and K. Held, Wien2wannier: From linearized augmented plane waves to maximally localized wannier functions, *Computer Physics Communications* **181**, 1888 (2010).
- [30] G. Jiang, C. Qin, K. Foyevtsova, L. Si, M. Berciu, G. A. Sawatzky, and M. Jiang, Intertwined charge and spin instability of $\text{La}_3\text{Ni}_2\text{O}_7$, *Science China Physics, Mechanics & Astronomy* **68**, 1 (2025).
- [31] H. Eskes, L. Tjeng, and G. Sawatzky, Cluster-model calculation of the electronic structure of CuO : A model material for the high- T_c superconductors, *Physical Review B* **41**, 288 (1990).
- [32] S. Sugano, Satoru Sugano, Y. Tanabe, and H. Kamimura, *Multiplets of transition-metal ions in crystals* (Elsevier, 2012).
- [33] M. Jiang, M. Berciu, and G. A. Sawatzky, Critical nature of the Ni spin state in doped NdNiO_2 , *Physical Review Letters* **124**, 207004 (2020).
- [34] J. Ghijsen, L. H. Tjeng, J. van Elp, H. Eskes, J. Westerink, G. A. Sawatzky, and M. T. Czyzyk, Electronic structure of Cu_2O and CuO , *Phys. Rev. B* **38**, 11322 (1988).
- [35] V. J. Emery and G. Reiter, Mechanism for high-temperature superconductivity, *Phys. Rev. B* **38**, 4547 (1988).
- [36] V. J. Emery and G. Reiter, Quasiparticles in the copper-oxygen planes of high- T_c superconductors: An exact solution for a ferromagnetic background, *Phys. Rev. B* **38**, 11938 (1988).
- [37] B. Lau, M. Berciu, and G. A. Sawatzky, High-spin polaron in lightly doped CuO_2 planes, *Phys. Rev. Lett.* **106**, 036401 (2011).
- [38] T. Mizokawa, D. I. Khomskii, and G. A. Sawatzky, Spin and charge ordering in self-doped mott insulators, *Phys. Rev. B* **61**, 11263 (2000).
- [39] J. Yang, J. Zhan, T. Miao, M. Huo, Q. Xu, Y. Li, Y. Xie, B. Liang, N. Cai, H. Chen, W. Zhu, M. Xu, S. Zhang, F. Zhang, F. Yang, Z. Wang, Q. Peng, H. Mao, X. Li, Z. Zhu, G. Liu, Z. Xu, J. Hu, X. Wu, M. Wang, L. Zhao, and X. J. Zhou, *Electronic origin of density wave orders in a trilayer nickelate* (2026), [arXiv:2601.22608 \[cond-mat.supr-con\]](https://arxiv.org/abs/2601.22608).
- [40] J. Zhang, D. Phelan, A. S. Botana, Y.-S. Chen, H. Zheng, M. Krogstad, S. G. Wang, Y. Qiu, J. A. Rodriguez-Rivera, R. Osborn, S. Rosenkranz, M. R. Norman, and J. F. Mitchell, Intertwined density waves in a metallic nickelate, *Nature Communications* **11**, 6003 (2020).
- [41] Z. Guan, S. F. TenHuisen, M. Tepie, Y. Zhao, E. Day-Roberts, H. LaBollita, A. M. Young, X. Cui, X. Chen, F. Glerean, *et al.*, Electronic layer decoupling driven by density-wave order in $\text{La}_4\text{Ni}_3\text{O}_{10}$, [arXiv preprint arXiv:2601.08997](https://arxiv.org/abs/2601.08997) (2026).